EurJIC
European Journal of Inorganic Chemistry

Research Article
doi.org/10.1002/ejic.202400078

Chemistry Europe
European Chemical Societies Publishing

www.eurjic.org

Enhancing the Analysis of Eu^{3+} Photoluminescence in Coordination Compounds in the Solid State by Determining their Refractive Index

Alexander E. Sedykh,*[a] Moritz Maxeiner,[a] Marcel T. Seuffert,[a] Dominik Heuler,[a] Dirk G. Kurth,[b] and Klaus Müller-Buschbaum*[a, c]

This study is focused on determining the refractive index as a crucial parameter for evaluating the intrinsic quantum yield and the ligand sensitisation efficiency in solid-state trivalent lanthanide coordination compounds. For this, eight trivalent europium complexes with phenyl-terpyridine ($[EuX_3(ptpy)(L)]$, X = Cl^- or NO_3^-, ptpy = 4′-phenyl-2,2′:6′,2″-terpyridine, L = H_2O or other molecules) were examined. Their refractive indices were determined using the Becke lines test by immersing transparent material in a series of media with known refractive indices. Using the set of media presented here, determining crystalline materials' refractive indices from 1.41 to 1.73 with a step of 0.01 is possible. Assessment of the refractive indices of the complexes mentioned above allowed a comprehensive analysis of their photophysical properties in the solid state. Moreover, this method can be extrapolated for other solid-state materials, offering valuable insights in the broader field of photophysics. In addition to photoluminescence investigations, the compounds presented were characterised by single-crystal X-ray diffraction (SCXRD), powder X-ray diffraction (PXRD), Hirschfeld surface area analysis, UV-Vis reflectance spectroscopy, hydrolysis sensitivity analysis, and simultaneous thermogravimetry and differential thermal analysis coupled with mass-spectrometry (STA-MS).

Introduction

Due to the characteristic 4f–4f luminescence of trivalent lanthanides, their compounds are widely investigated as phosphors. Photoluminescence properties of Ln^{3+} are generally studied in inorganic[1–3] or coordination compounds.[4–11] Furthermore, these metal ions could be used as dopants[12–16] or embedded in polymeric films.[17–21] In suitable coordination compounds, the organic ligand acts as an "antenna" for the sensitisation of Ln^{3+} luminescence, being beneficial due to the low light uptake of lanthanide ions employing intra-4f-transitions.[22,23] Thereby, the ligand is used to harvest the light, typically in the UV region, and to transfer energy to the emissive metal ion, increasing the brightness of their photoluminescence.[22–24]

The red luminescence of trivalent europium has a wide variety of applications. It is used in $Y_2O_3:Eu^{3+}$ phosphor in fluorescent lamps.[25] With the development of the technology, complexes and inorganic compounds of Eu^{3+} started to be implemented in light-emitting diodes (LEDs), either as a red-emitting LED[26–28] or as a part of a white-emitting LED.[28–30] Eu^{3+}-containing LEDs could be used as vapoluminescent sensors with a recyclable on–off–on luminescence.[28] The response of Eu^{3+} complexes to pH could also be used for anti-counterfeiting purposes.[31,32] Even in general, the red luminescence of trivalent europium is usable for authentication when implemented in a security label.[33,34] The europium is even used for this purpose in euro banknotes.[25,35] Eu^{3+}-luminescence is broadly used in luminescence thermometry,[36,37] which then could be used for temperature mapping of tissue[38,39] or, again, for anti-counterfeiting purposes.[40] Understanding luminescence efficiency is crucial to developing better materials for the applications mentioned.

The expanding research on trivalent lanthanide compounds generates additional interest in evaluating their quantitative photophysical properties (quantum yield and lifetime), also in the solid state. Besides direct measurement of quantum yield and lifetime, assessment of radiative and non-radiative processes within the compounds is beneficial for a better understanding of their photoluminescence and further materials' development. For Eu^{3+}-containing compounds, calculating

[a] Dr. A. E. Sedykh, M. Maxeiner, M. T. Seuffert, D. Heuler, Prof. Dr. K. Müller-Buschbaum
Institute of Inorganic and Analytical Chemistry
Justus-Liebig-University Giessen
Heinrich-Buff-Ring 17, 35392 Giessen, Germany
E-mail: alexander.sedykh@ac.jlug.de
kmbac@uni-giessen.de
Homepage: www.uni-giessen.de/fbz/fb08/Inst/iaac/mueller-buschbaum

[b] Prof. Dr. D. G. Kurth
Lehrstuhl für Chemische Technologie der Materialsynthese
Julius-Maximilians-Universität Würzburg
Röntgenring 11, 97070 Würzburg, Germany

[c] Prof. Dr. K. Müller-Buschbaum
Center for Materials Research (LAMA)
Justus-Liebig-University Giessen
Heinrich-Buff-Ring 16, 35392 Giessen, Germany

Supporting information for this article is available on the WWW under https://doi.org/10.1002/ejic.202400078

Research Article
doi.org/10.1002/ejic.202400078

radiative and non-radiative process constants is an established procedure.[41] It involves utilising experimental values of observed quantum yield (Φ_{obs}) and lifetime (τ_{obs}) in conjunction with an emission spectrum. First, evaluation of a radiative lifetime τ_{rad} (s) or radiative process rate constant k_{rad} (s^{-1}) is required, which can be calculated according to Werts' formula (Eq. 1):[41]

$$\frac{1}{\tau_{rad}} = k_{rad} = A_{MD,0} n^3 \left(\frac{I_{tot}}{I_{MD}}\right) \quad (1)$$

where $A_{MD,0}$ is the spontaneous emission probability for the $^5D_0 \rightarrow {}^7F_1$ transition in vacuum (14.65 s^{-1}),[41] n is the refractive index of the medium, I_{tot} is the integrated emission intensity of $^5D_0 \rightarrow {}^7F_J$ ($J = 0$–6) transitions, and I_{MD} is the integrated emission intensity of $^5D_0 \rightarrow {}^7F_1$ transition. Typically, the transitions $^5D_0 \rightarrow {}^7F_5$ (~13300 cm^{-1}, 750 nm) and $^5D_0 \rightarrow {}^7F_6$ (~12300 cm^{-1}, 815 nm) are of low intensity or may even not be observed due to the detector's low sensitivity at the edge of the NIR region. As this limits their overall impact strongly, they may be omitted from the calculation of the radiative process.[25]

Knowing the radiative process value, calculation of the intrinsic quantum yield Φ_{Ln} and non-radiative de-excitation constant k_{nrad} (s^{-1}) from the observed lifetime τ_{obs} and radiative lifetime τ_{rad} is possible according to (Eq. 2):[41]

$$\Phi_{Ln} = \frac{k_{rad}}{k_{rad} + k_{nrad}} = \frac{\tau_{obs}}{\tau_{rad}} \quad (2)$$

The efficiency of a ligand's "antenna" effect can also be evaluated. The sensitisation efficiency η_{sens} of the ligand is calculated as the ratio of the observed quantum yield Φ_{obs} and the intrinsic quantum yield (Φ_{Ln}) (Eq. 3):[41]

$$\eta_{sens} = \frac{\Phi_{obs}}{\Phi_{Ln}} \quad (3)$$

The refractive index n is used not only included in the Werts' formula (Eq. 1),[41] but also in the calculations according to the Judd-Ofelt theory,[42,43] which is applicable to all Ln^{3+}-ions with 4f–4f-based luminescence. For Ln^{3+}-doped materials like glasses or polymer films, it is possible to use a refractive index value either measured directly or acquired from the literature. In the context of solid-state Ln^{3+} coordination compounds, the refractive index value is commonly approximated, often as 1.50[44–52] or 1.55[53,54] for the calculation of radiative lifetime (Eq. 1). While this approximation is generally effective, it can lead to unwanted discrepancies. This practice may result in an observed quantum yield Φ_{obs} exceeding the calculated intrinsic quantum yield Φ_{Ln} in certain cases.[45–47,55] Such instances imply a sensitisation efficiency η_{sens} greater than 100%, which is typically unfeasible. Although these observations suggest the nearly quantitative sensitisation efficiency of the ligand, they also highlight a potential area for refinement in the evaluation of Φ_{Ln} and η_{sens}. A determination of the refractive index, therefore, enhances the assessment of these values.

In this work, we study eight complexes of the general formula $[EuX_3(ptpy)(L)]$ ($X = Cl^-$ or NO_3^-, ptpy = 4′-phenyl-2,2′:6′,2″-terpyridine, $L = H_2O$ or organic molecule). Notably, for seven of these complexes, approximating the refractive index value as 1.5 would also lead to Φ_{obs} being higher than Φ_{Ln}. The current study includes both a revisit of a previously reported complex and the introduction of new compounds. Among complexes with a composition of $[EuX_3(ptpy)(L)]$, some are already known in the literature: $[EuCl_3(ptpy)(py)]$,[56] $[EuCl_3(ptpy)(acetamide)]$,[57] and α-$[Eu(NO_3)_3(ptpy)(H_2O)]$ (**1**).[45] Here, the properties of complex **1** are re-evaluated for a more insightful comparison. Additionally, we introduce several novel compounds, namely β-$[Eu(NO_3)_3(ptpy)(H_2O)]$ (**2**), $[Eu(NO_3)_3(ptpy)(acetone)]$ (**3**), $[Eu(NO_3)_3(ptpy)(thf)]$ (**4**), $[Eu(NO_3)_3(ptpy)(MeOH)]$ (**5**), $[EuCl_3(ptpy)(acetone)]$ (**6**), $[EuCl_3(ptpy)(thf)]$ (**7**), and $[EuCl_3(ptpy)(MeOH)]$ (**8**). The refractive indices of these compounds were determined using the Becke lines test[58,59] to enhance the understanding of their photoluminescence characteristics. By assessing the quantitative photophysical properties of these compounds in the solid state, it is possible to more precisely ascribe the effects of crystal structure and coordination environment on the Eu^{3+} photoluminescence.

Results and Discussion

Excitation and emission spectra of $[EuX_3(ptpy)(L)]$ (**1**–**8**) were determined in the solid state at room temperature and are presented in Figure 1. A broad ligand-based band dominates the excitation spectra, and emission spectra exhibit the characteristics of Eu^{3+} transitions $^5D_0 \rightarrow {}^7F_J$ ($J = 0$–4) with a Stark splitting of the energy levels and relative intensities typical for a low symmetry local geometry,[25,60] which correlates with the crystallographic data. The transition $^5D_0 \rightarrow {}^7F_0$ (580–582 nm, ~17200 cm^{-1}) is observed for all complexes **1**–**8**, which indicates that the coordination sphere of Eu^{3+} has either C_{nv}, C_n or C_s symmetry.[25] The magnetic dipole transition $^5D_0 \rightarrow {}^7F_1$ (588–602 nm, ~16800 cm^{-1}) could potentially be split into three lines, as the degeneracy of each spin-orbit ^7F_J level is $2J + 1$.[25] For complexes **7** and **8**, three lines could be observed directly. In contrast, for **1**–**6**, only two lines are cleanly distinguishable as a result of low splitting energy and insufficient resolution due to the temperature effect. Three lines of $^5D_0 \rightarrow {}^7F_1$ transition together with the presence of $^5D_0 \rightarrow {}^7F_0$ limit possible point groups of Eu^{3+} centre to C_1, C_s, C_2, and C_{2v}.[25] Two lines observed for the $^5D_0 \rightarrow {}^7F_1$ transition could expand the list by C_n and C_{nv} with $n = 3$, 4, or 6.[25] The hypersensitive transition $^5D_0 \rightarrow {}^7F_2$ (610-630 nm, ~16200 cm^{-1}) could be split into a maximum of five lines. For **4** and **6**–**8**, four lines are observed for this transition, with a small additional shoulder being noticeable. Three lines of the transition $^5D_0 \rightarrow {}^7F_2$ are observed for **1**, **2**, **3** (with one shoulder), and **5** (with two shoulders). Even three lines present for this transition exclude C_n and C_{nv} with $n = 4$ or 6 point groups of Eu^{3+} local symmetry for all compounds, given previously described observations of emission spectra.[25] Transition $^5D_0 \rightarrow {}^7F_3$ (640–665 nm, ~15400 cm^{-1}) is of low intensity for compounds **1**–**8**, as typical for Eu^{3+}

Research Article
doi.org/10.1002/ejic.202400078

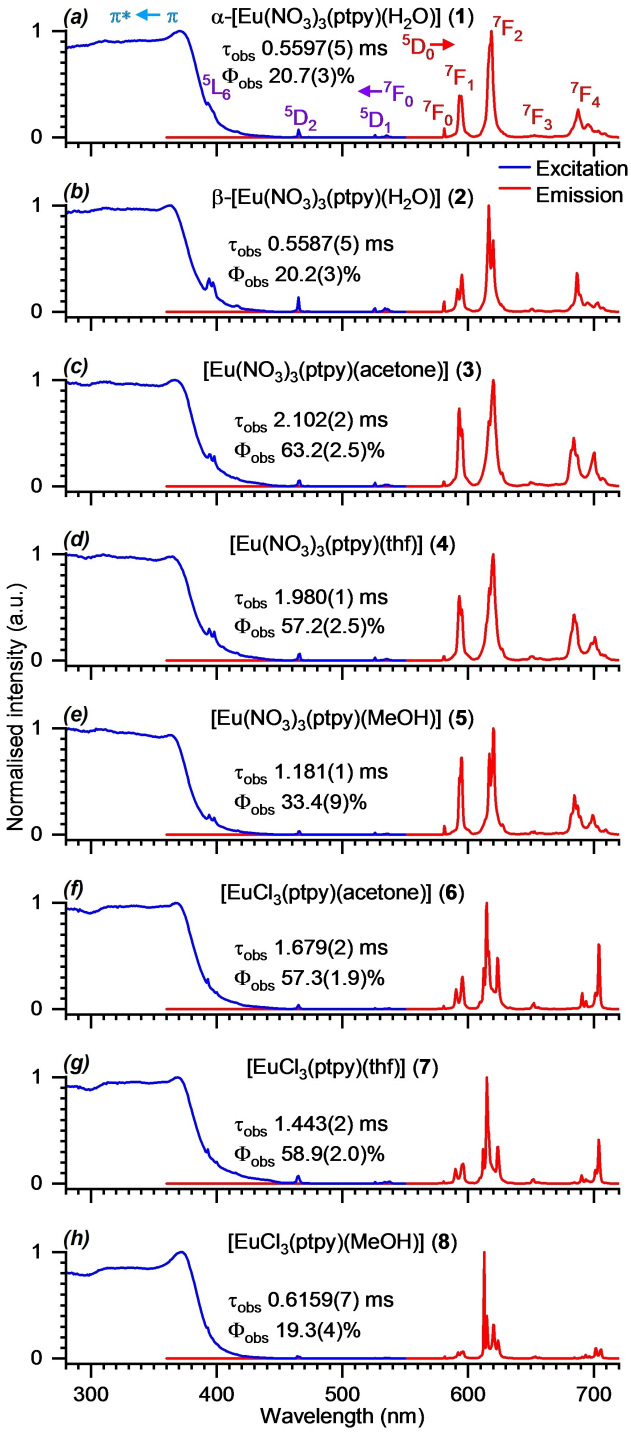

Figure 1. Room temperature solid state normalised excitation (blue, transition $^5D_0 \rightarrow {}^7F_2$ was monitored) and emission spectra (red, $\lambda_{ex} = 350$ nm) of **1**–**8**. Observed lifetime (τ_{obs}) and quantum yield (Φ_{obs}) values are presented. Exemplarily for (a), the ligand-based excitation transition is marked in light blue, direct Eu^{3+} excitation transitions are identified and indicated in violet, and Eu^{3+} emission transitions are in red.

luminescence, and therefore of little use for analysing coordination sphere symmetry. The last recorded transition $^5D_0 \rightarrow {}^7F_4$ (675–715 nm, ~14500 cm^{-1}) is split into nine lines for **1** and **3**, eight lines for **4**, **5**, and **8**, seven lines for **2**, six lines for **7**, and only five distinguishable lines for **6**. The cross-elimination of possible options reduces the possible local symmetry for Eu^{3+} to C_1, C_s, C_2 for **1**, **3**–**5**, and **8**, with an expansion of C_{2v} for **2**, **6**, and **7**. The crystallographically determined symmetry of Eu^{3+} coordination sphere in complexes **1**–**8** is, in all cases, C_1, being close to C_s.

Solid-state UV-Vis spectra were also recorded and are in good agreement with the excitation spectra for compounds **1**–**8**. The products obtained absorb 60–85% of the light in the UV region from 200 to 375 nm. Absorption by direct Eu^{3+} transitions ($^5L_6 \leftarrow {}^7F_0$ (397 nm), $^5D_2 \leftarrow {}^7F_0$ (465 nm), and $^5D_1 \leftarrow {}^7F_0$ (535 nm)) are lower in amplitude than the ligand-based absorption, also being observed in the excitation spectra (Figure 1). Solid-state reflectance spectra for products **1**–**8** are presented in the SI (Figure S1). Complex units of **3** and **6** are exemplarily shown in Figure 2.

Measured quantum yield (Φ_{obs}) and lifetime (τ_{obs}) values for complexes **1**–**8** are presented in Table 1 as well as in Figure 1. Additionally, ratios of integrated intensities I_{tot}/I_{MD}, derived from the emission spectra, are presented in Table 1. With these three experimental photoluminescence parameters at hand, it is possible to evaluate radiative lifetime (τ_{rad}), intrinsic quantum yield (Φ_{Ln}), and ligands' sensitisation efficiency (η_{sens}) for **1**–**8** according to Eq. 1–3. However, approximating the refractive index as 1.5 in Eq. 1 (for calculation of radiative lifetime τ_{rad}) leads to ambiguous results. Specifically, for compounds **1**–**7**, this approximation results in an experimental value Φ_{obs} being higher than calculated from Eq. 2 Φ_{Ln}, which is commonly unreasonable from the photophysical perspective. It must be noted that this observation of the measured quantum yield Φ_{obs} being consistently higher than the intrinsic quantum yield Φ_{Ln} for these complexes is not due to Φ_{obs} measurement inaccuracies. This is corroborated by the fact that, for the literature-known complex **1**, a similar pattern is observed where Φ_{obs} exceeds Φ_{Ln}, as previously reported Φ_{obs} is 16.8% and Φ_{Ln} is 14.6%.[45] The slight discrepancy in the exact Φ_{obs} values

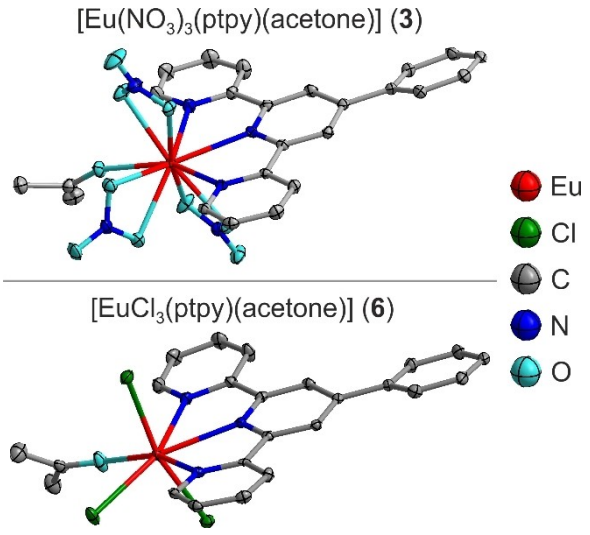

Figure 2. Excerpts of the X-ray crystal structures displaying a complex unit of $[Eu(NO_3)_3(ptpy)(acetone)]$ (**3**, top) and $[EuCl_3(ptpy)(acetone)]$ (**6**, bottom), respectively. Thermal ellipsoids depict a 50% probability level of the atoms (Eu red, Cl green, C grey, N blue, O light blue, hydrogen atoms are omitted).

Research Article
doi.org/10.1002/ejic.202400078

Chemistry Europe
European Chemical Societies Publishing

Table 1. Room temperature solid-state quantitative photophysical data of **1**–**8**.

Compound	τ_{obs} (ms)[a]	Φ_{obs} (%)[b]	I_{tot}/I_{MD}[c]	n[d]	τ_{rad} (ms)[e]	k_{rad} (s^{-1})[f]	k_{nrad} (s^{-1})[g]	Φ_{Ln} (%)[h]	η_{sens} (%)[i]
α-[$Eu(NO_3)_3$(ptpy)(H_2O)] (**1**)	0.5597(5)	20.7(3)	5.74	1.71	2.38	420	1366	24	86
β-[$Eu(NO_3)_3$(ptpy)(H_2O)] (**2**)	0.5587(5)	20.2(3)	6.20	1.69	2.28	438	1351	24	84
[$Eu(NO_3)_3$(ptpy)(acetone)] (**3**)	2.102(2)	63.2(2.5)	5.05	1.64	3.06	327	149	69	92
[$Eu(NO_3)_3$(ptpy)(thf)] (**4**)	1.980(1)	57.2(2.5)	5.33	1.68	2.70	370	135	73	78
[$Eu(NO_3)_3$(ptpy)(MeOH)] (**5**)	1.181(1)	33.4(9)	4.72	1.70	2.94	340	507	40	84
[$EuCl_3$(ptpy)(acetone)] (**6**)	1.679(2)	63.2(9)	6.37	1.71	2.14	467	129	78	81
[$EuCl_3$(ptpy)(thf)] (**7**)	1.516(2)	58.9(2.0)	6.82	1.69	2.07	482	177	73	81
[$EuCl_3$(ptpy)(MeOH)] (**8**)	0.6805(6)	19.3(4)	9.82	1.64	1.58	635	835	43	45

[a] Observed luminescence lifetime excited by a microsecond flash lamp at 350 nm, emission maximum of transition $^5D_0 \rightarrow {}^7F_2$ was monitored. [b] Observed photoluminescence quantum yield, $\lambda_{ex} = 350$ nm, $\lambda_{em} = 575$–720 nm. [c] Ratio of integrated emission intensity of $^5D_0 \rightarrow {}^7F_J$ ($J = 0$–4) transitions to integrated emission intensity of $^5D_0 \rightarrow {}^7F_1$ transition. [d] Refractive index. [e] Radiative lifetime calculated according to Eq. 1, transitions $^5D_0 \rightarrow {}^7F_J$ ($J = 0$–4) were integrated for evaluation of I_{tot}. [f] Radiative process constant calculated according to Eq. 1. [g] Non-radiative process constant calculated according to Eq. 2. [h] Intrinsic quantum yield calculated according to Eq. 2. [i] Sensitisation efficiency calculated according to Eq. 3.

between the literature and our current determinations can be attributed to differences in the instrumental setup. Importantly, both in our study and in the literature example, Φ_{obs} is found to be higher than Φ_{Ln} for complex **1** when approximating a refractive index as 1.5 in the calculations.

To address the issue of refractive index value used in the photophysical parameters' calculations, the refractive indices of complexes **1**–**8** were determined using the Becke lines test.[58,59] According to this method, crystals of the compound in question are immersed in a liquid with a known refractive index. The behaviour of light transmitted through the transparent sample is analysed with a microscope. Refraction and reflection of light at the edge of the crystal give rise to the so-called Becke lines, as schematically presented in Figure 3. The Becke-lines are most prominent if the index of refraction of the liquid and the crystal is large and will faint as both refractive indices become equal.[58] Upon increasing the focal distance, the Becke lines move towards the medium that has the higher refraction index, that is either towards the crystal ($n_{crystal} > n_{medium}$) or the medium ($n_{crystal} < n_{medium}$).[59] See SI Video for a visual presentation of this effect. Analysing the compound in several media with gradually changing refractive indices makes it possible to evaluate its refractive index. It is determined as being in between the refractive indices of two media adjacent in the series, for which the reversal of the Becke lines' behaviour is observed. For this work, combinations of 1-chlorobutane:1,2-dichlorobenzene, 1,2-dichlorobenzene:1-bromonaphthalene, and 1-bromonaphthalene:diiodomethane were selected with molar ratios from 0 to 1. These mixtures have refractive indices from 1.401 to 1.734 (Table S1 and Figure S2). Using these media, determining the refractive index of solid-state crystalline compounds is possible in a range from 1.41 to 1.73 with a step of 0.01.

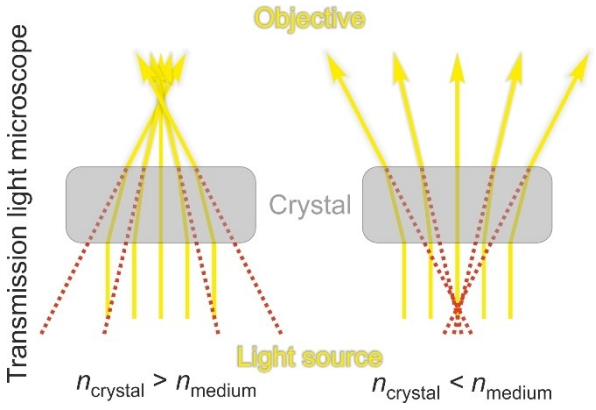

Figure 3. Schematic illustration of Becke lines' formation at the crystal's interface with higher refractive index (left) and lower refractive index (right) than the medium, as observed in the transmission light microscope. The solid yellow lines represent the path of light through the crystals. The red dashed lines indicate the perceived position of the Becke lines relative to the crystal boundary. See SI Video for a visual presentation of Becke lines' behaviour for a crystal in three different media upon increasing the focal distance.

After the determination of refractive indices for **1**–**8** and with the other photoluminescence properties being known, an evaluation of the radiative lifetime (τ_{rad}), intrinsic quantum yield (Φ_{Ln}), and ligands' sensitisation efficiency (η_{sens}) can be done according to Eq. 1–3. The results of these calculations are presented in Table 1. Now, we can exactly compare the Eu^{3+} luminescence parameters of complexes **1**–**8** depending on the molecular and crystal structure. Quantum yield (both Φ_{Ln} and Φ_{obs}) and observed lifetime values are several times lower for compounds **1** and **2** compared to the other complexes presented here (Table 1). This results from quenching by O–H vibrations of the water molecule coordinated to the metal ion. Participation of a non-radiative process is significant for both **1** and **2** ($k_{nrad} > 1350$, Table 1). In contrast, complexes with an aprotonic organic molecule coordinated to Eu^{3+} (acetone in **3** and **5**, tetrahydrofuran in **4** and **7**) have high intrinsic quantum yield values Φ_{Ln}, 69–78% (Table 1). The energy transfer from the ligand to the emissive metal ion is also efficient (η_{sens} 78–92%, Table 1). As a result, complexes **3**–**5** and **7** have high observed quantum yields of 57–63% (Table 1). For both complexes containing MeOH coordinated to the metal ion, the values of Φ_{Ln} are close to one another, 40% for **5** and 43% for **8**. The quenching effect of MeOH is not as strong as for the water

Research Article
doi.org/10.1002/ejic.202400078

molecule, observed for Ln^{3+} complexes before.[10] A lower Φ_{obs} for **8** (19.3(4) %) than for **5** (33.4(9) %) is the result of the lower ligand sensitisation efficiency. For complexes **1**–**7**, η_{sens} is between 78 and 92 % (Table 1), while for product **8** it is 45 %.

An analysis of the crystal structure should be helpful to answer the arising question of why the same ligand within the complexes of the general composition $[EuX_3(ptpy)(L)]$ shows such a drastic difference in sensitisation of Eu^{3+}-luminescence. The overall photoluminescence efficiency of Ln^{3+} coordination compounds depends on the triplet state energy of the sensitiser ligand.[61] Energies of electronic states for the same organic moiety – especially aromatic systems – depend on the crystal packing.[62] Estimating energetic state energies for solid-state materials using quantum mechanical calculations is still a computational challenge, even more so for lanthanide-containing materials. Nonetheless, differences in the crystal structure of chemically similar complexes **1**–**8** can be analysed.

In the nitrate-containing complexes **1**, **2**, **4**, and **5**, the europium ion has the coordination sphere of a distorted gyroelongated square bipyramid (CN 10). In $[Eu(NO_3)(ptpy)(acetone)]$ (**3**), the coordination sphere of the metal ion is a distorted sphenocorona (CN 10).[63] Chloride-containing complexes **6**–**8** have a coordination sphere of a distorted pentagonal bipyramid (CN 7). For all compounds reported, see SI Tables S2–S4 for crystallographic data and SI Tables S5–S11 for details on the Eu^{3+} coordination sphere. X-ray crystal structures of a complex unit and coordination polyhedra are presented in SI Figures S3–S9. The coordination environments cannot explain the difference in ligand's sensitisation efficiency between **8** and complexes **1**–**7**. Therefore, the crystal packing of molecular units was analysed.

Complexes **2**–**7** are isostructural, crystallising in the space group *Pbca*, with dimensions of a unit cell *a*, *b*, and *c* axes being dependent on the size of the anion (chloride or nitrate) and organic molecule being co-coordinated alongside ptpy. α-$[Eu(NO_3)_3(ptpy)(H_2O)]$ (**1**) also crystallises in the space group *Pbca*, though with a different crystal packing. $[EuCl_3(ptpy)(MeOH)]$ (**8**) crystallises in the triclinic space group $P\bar{1}$. For complex α-$[Eu(NO_3)_3(ptpy)(H_2O)]$ (**1**), a crystal packing analysis is already presented in the literature.[45] As complexes **2**–**7** are isostructural, $[EuCl_3(ptpy)(acetone)]$ (**6**) (Figure 4) is exemplarily compared to $[EuCl_3(ptpy)(MeOH)]$ (**8**) (Figure 5). Complexes **2**–**7** form infinite 2D layers of complex units over π–π stacked ligands (Figure 4). Only two contacts are present, with the Hirschfeld surface analysis of the C···C contacts showing short intermolecular contacts (Figure 4, Contact 1, red dots) being smaller than the sum of van der Waals radii. In contrast, complex **8** has five short intermolecular C···C contacts (Figure 5) with a way more complicated π–π stacking packing scheme that extends in all three dimensions. Participation of C···C intermolecular contacts is much higher for complex **8** (10.3 %) than for compounds **1**–**7** (6.5–7.9 %). A summary of the participation of intermolecular contacts in their distribution by elements for all complexes **1**–**8** is provided in the SI (Table S12). While it is challenging to conclusively determine how the crystal packing influences the energy states of the "antenna" ligand in complexes **1**–**8**, there is an indication that in this particular case of an increase in intermolecular contacts among ligands coupled with an extension of the π–π stacking in all dimensions, reduces the efficiency of the energy transfer from the ligand to Eu^{3+}.

Complexes $[EuX_3(ptpy)(L)]$ (**1**–**8**) were obtained directly from a reaction between the corresponding europium salt hydrate and ptpy (Scheme 1). If acetone, tetrahydrofuran, or methanol are used, they coordinate to the metal centre. If acetonitrile is used, a water molecule is coordinated. Two modifications of

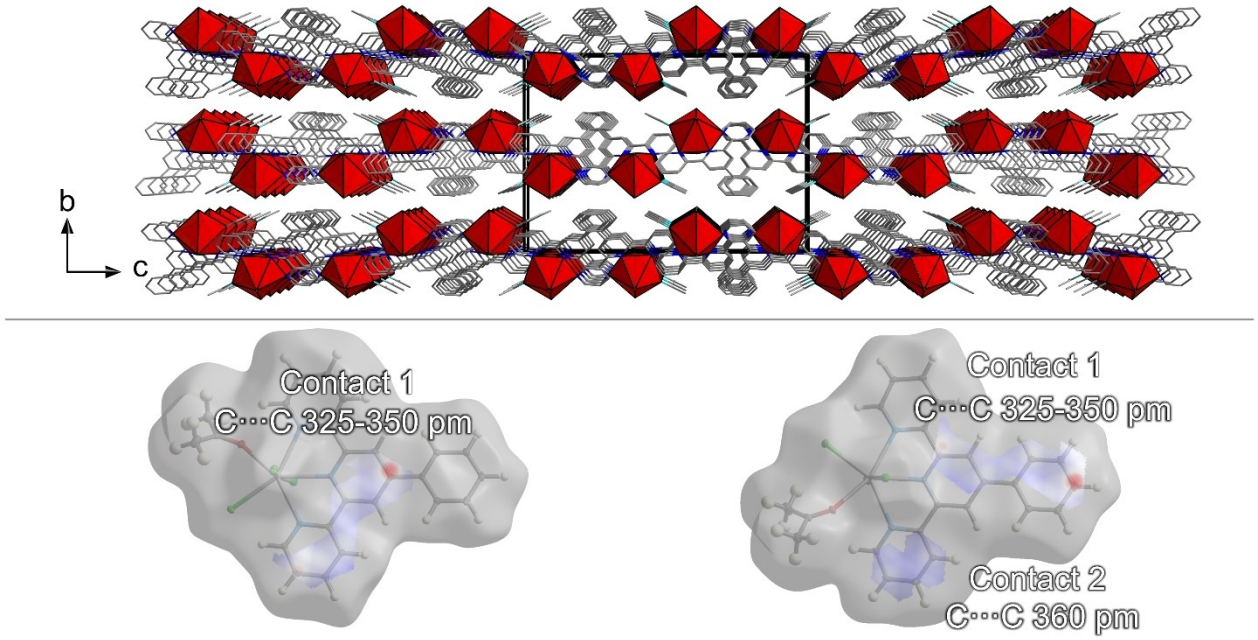

Figure 4. Top: X-ray crystal structure of $[EuCl_3(ptpy)(acetone)]$ (**6**) shown along the *a* axis, illustrating 2D-layers formed by π–π stacking. Bottom: Hirschfeld surface of $[EuCl_3(ptpy)(acetone)]$ (**6**), mapped over d_{norm} (−0.1734 to 1.3273 a.u.), with only C···C intermolecular contacts shown.

Research Article
doi.org/10.1002/ejic.202400078

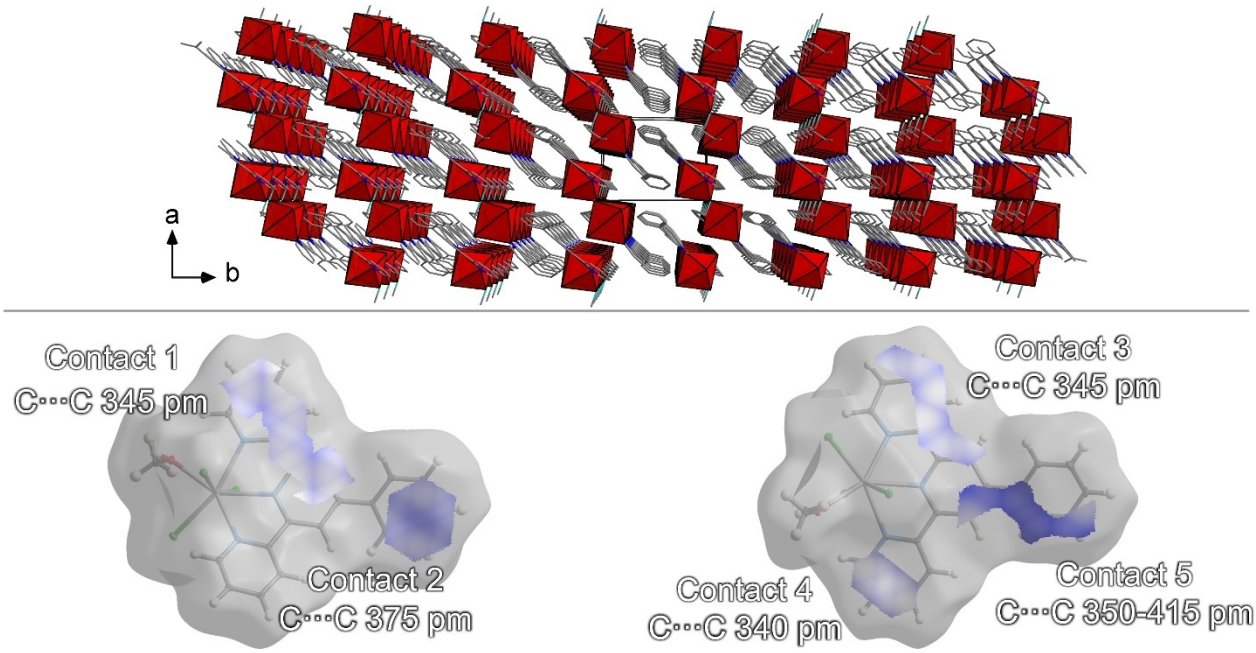

Figure 5. Top: X-ray crystal structure of $[EuCl_3(ptpy)(MeOH)]$ (**8**) shown along the *c* axis. Bottom: Hirschfeld surface of $[EuCl_3(ptpy)(MeOH)]$ (**8**), mapped over d_{norm} (−0.4405 to 1.1788 a.u.), with only C···C intermolecular contacts shown.

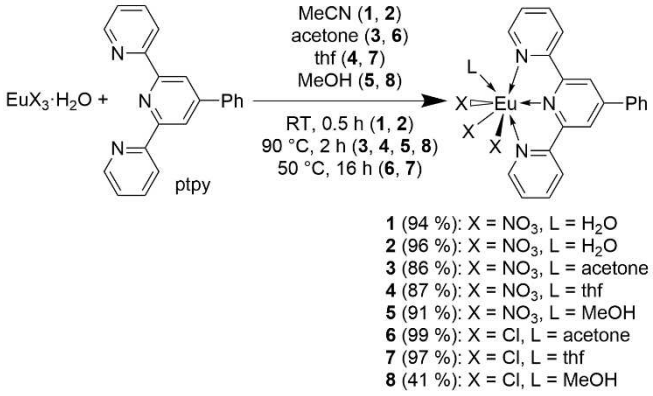

Scheme 1. Synthesis of $[EuX_3(ptpy)(L)]$ (**1**–**8**).

$[Eu(NO_3)_3(ptpy)(H_2O)]$ were observed: alpha (**1**), reported before,[45] and a previously unreported beta phase (**2**). During our studies, under the same reaction conditions (room temperature, 0.5–2 h), both compounds were obtained. At elevated temperatures (up to 80 °C), only α-$[Eu(NO_3)_3(ptpy)(H_2O)]$ (**1**) was obtained. Originally, it was also reported to be obtained from acetonitrile at 80 °C.[45] Five further complexes, $[Eu(NO_3)_3(ptpy)(MeCN)]$ (**9**), $[Eu_2(NO_3)_6(ptpy)_2]$ (**10**), $[Eu(NO_3)_3(ptpy)(H_2O)]\cdot thf$ (**11**), $[EuCl_3(ptpy)(H_2O)(MeOH)]$ (**12**), and $[EuCl_2(ptpy)_2]Cl\cdot 2MeOH$ (**13**), were successfully isolated but only as single crystals. They can be ascribed as possible intermediates or byproducts in the synthesis of the complexes $[EuX_3(ptpy)(L)]$. Comparison of measured and simulated powder X-ray diffractograms (PXRD) is presented in the SI (Figures S10–S17).

The thermal properties of compounds **1**–**8** were investigated by simultaneous thermogravimetry and differential thermal analysis coupled with mass-spectrometry (STA-MS). Phase transitions during the heating were analysed *in situ* using temperature-dependent powder X-ray diffraction (PXRD) as an additional experimental method. Upon heating, the coordinated water or organic solvent molecule is released at 150–240 °C; the exact release temperature depends on the compound (Figure S18). Therefore, these compounds show thermal properties corroborating the previously reported compounds $[EuCl_3(ptpy)(py)]$ and $[EuCl_3(ptpy)(acetamide)]$.[57] After the release of the smaller ligand, nitrate complexes **1**–**5** form dimeric complex $[Eu_2(NO_3)_6(ptpy)_2]$ (**10**), independent of the initial complex packing (see SI Figures S19 and S20 for temperature-dependant PXRD investigations of **1** and **2**). Dimer **10** decomposes at 350 °C with a release of nitric oxides and the ptpy ligand being partially oxidised, forming Eu_2O_3 and organic decomposition products. Chloride-containing complexes **6** and **7** form an amorphous compound after the release of acetone or thf, respectively (see SI Figure S21 for temperature-dependent PXRD investigations of **7**). Similarly to previously presented isostructural $[EuCl_3(ptpy)(py)]$,[56] products **6** and **7** undergo an exothermic phase transition at 315 °C to an unidentified crystalline compound. $[EuCl_3(ptpy)(MeOH)]$ (**8**) already forms the same unknown crystalline compound directly after the methanol release (see SI Figure S22 for temperature-dependent PXRD investigations of **8**). For all chloride-containing complexes **6**–**8**, the solvent-free form subsequently decomposes at 470 °C.

Out of complexes **1**–**8**, only $[Eu(NO_3)_3(ptpy)(H_2O)]$ (**1** and **2**) are stable on air against humidity. Complexes with nitrate anions (**3**–**5**) show an exchange of coordinated solvent molecules to water, forming β-$[Eu(NO_3)_3(ptpy)(H_2O)]$ (**2**) with poor crystallinity. Complexes with chloride anions (**6**–**8**) are hydrolysed completely, with ptpy removed from the Eu^{3+} coordination sphere. Since this leads to significant lumines-

Research Article
doi.org/10.1002/ejic.202400078

cence loss, this property could be used for irreversible humidity sensing.[64]

Conclusions

Eight complexes of the general constitution $[EuX_3(ptpy)(L)]$ (X = Cl^- or NO_3^-, ptpy = 4′-phenyl-2,2′:6′,2″-terpyridine, L = H_2O or organic molecule) are presented. Using these compounds as model compounds, the benefit of determining the refractive index for calculating quantitative photoluminescence values, namely intrinsic quantum yield and ligand sensitisation efficiency, was deliberately analysed. The refractive indices were determined using the Becke lines test, an immersion method. A series of binary organic liquid systems used as media for the sample immersion are presented. The analyte's refractive index is determined as being between the refractive indices of two media with adjacent refractive indices, for which the behaviour of the sample Becke lines' is the opposite. The set of media used in this work allows the evaluation of a crystalline compound's refractive index from 1.41 to 1.73 with a step of 0.01. Determination of the refractive index value for solid-state crystalline compounds allows the calculation of the radiative lifetime of 4f–4f luminescence of Ln^{3+} according to Judd-Ofelt theory in general and of Eu^{3+} according to Werts' formula in particular. With the radiative lifetime being assessed, further photoluminescence parameters representing the luminescence performance, namely intrinsic Eu^{3+} quantum yield and ligand sensitisation efficiency, were evaluated. Therefore, determining various aspects' influence on the system's photoluminescence performance is possible. Crystal packing and luminescence quenching by co-coordinated solvent molecules are examples of these factors and were evaluated for the model compounds presented.

Supporting Information

Deposition Numbers 2236754 (for **1**), 2236755 (for **2**), 2236756 (for **3**), 2236757 (for **4**), 2236758 (for **5**), 2236759 (for **6**), 2236760 (for **7**), 2236761 (for **8**), 2236762 (for **9**), 2236763 (for **10**), 2236764 (for **11**), 2236765 (for **12**), and 2236766 (for **13**) contain the supplementary crystallographic data for this paper. These data are provided free of charge by the joint Cambridge Crystallographic Data Centre and Fachinformationszentrum Karlsruhe Access Structures service.

The Supporting Information (22 pages) contains tables with crystallographic data, selected interatomic distances and angles, and powder X-ray diffraction plots. The authors have cited an additional reference within the Supporting Information.[65] Normalised excitation and emission spectra, UV-Vis reflectance spectra, powder X-ray diffraction data, and thermal analysis data of compounds **1**–**8** are available at the data repository of Justus-Liebig-University Gießen JLUpub under https://doi.org/10.22029/jlupub-18225. An example of Becke lines' behaviour is presented in the SI video for sodium acetate trihydrate (*n* 1.464)[66] cojoined crystals in three different media (air with *n* 1.0003, a mixture of limonene and n-hexane with *n* 1.462, 1-bromonaphtalene with *n* 1.656).[67,68]

Experimental

$Eu(NO_3)_3 \cdot 6H_2O$, $EuCl_3 \cdot 6H_2O$ (both 99.9 %, abcr), acetonitrile (> 99 %), dry acetone, dry methanol (both 99.8 %, AcroSeal, Thermo Scientific), and dry tetrahydrofuran (99.5 %, AcroSeal, Thermo Scientific) were used as received. 4′-phenyl-2,2′:6′,2″-terpyridine (ptpy) was synthesised from benzaldehyde and 2-acetylpyridine as described in the literature.[69] Duran® culture tubes (12×100 mm, test tubes with a screw cap), Duran® glass ampoules (outer ø 10 mm, wall thickness 1.5 mm), and special quick-fits for their connection to the vacuum line were used for the synthesis. Products were stored and prepared for analysis inside a glovebox (MBRAUN LABmaster SP).

Photoluminescence Investigations. Excitation and emission spectra were recorded using the FluoroEssence software on a Fluorolog 3 spectrometer (HORIBA) equipped with a dual lamp house, Xe short-arc lamp (USHIO, 450 W), Xe short-arc flashlamp (Excelitas FX-1102, average power 10 W), double-grated monochromators, a photomultiplier detector (R928P), and a TCSPC upgrade. Spectra were corrected for the spectral response of monochromators and detector using correction files provided by the manufacturer. Excitation spectra were additionally corrected for the lamp's spectral distribution using the reference photodiode detector. A long-pass filter (Newport, cut-off wavelength 495 nm) was used to avoid second-order light reflection by monochromators. Overall emission decay times were measured on the same setup using the DataStation software. A microsecond flashlamp was used for the excitation. The overall emission intensity decay was fitted with the mono-exponential decay function $I(t) = A + B \cdot e^{(-t/\tau)}$ using the Decay Analysis Software 6.

For the determination of quantum yield values, another Fluorolog 3 (HORIBA) was used, equipped with a Xe short-arc lamp (USHIO, 450 W), double-grated monochromators, a photomultiplier detector (R928P), and a Quanta-Phi Integrating Sphere (HORIBA). The setup for quantum yield measurements was double-checked by measuring several solid-state photoluminescence standards: sodium salicylate (53.4(2.0), lit.: 53–57 %),[70,71] γ-$[Tb_4(OAc)_{12}(ptpy)_2]$ (measured: 44.8(9) %; lit.: 46 %),[72] and γ-$[Eu_4(OAc)_{12}(ptpy)_2]$ (measured: 57.8(6) %; lit.: 58–62 %).[72] Solid samples were filled in a micro cell quartz cuvette (Starna 18-F/ST/C/Q/10; fluorescence with ST/C closed-cap, material UV quartz glass Spectrosil Q, pathlength 10 mm, matched). A cuvette filled with magnesium oxide was used as reference material. Each sample was measured several times, and the average quantum yield with a standard deviation was calculated from these measurements. Standard deviations represent the measurement error. The actual error of the method can be as high as 20 % of the given quantum yield value.

Refractive Index Determination. The refractive indices of organic solvents and their binary mixtures were determined at 24 ± 1 °C using an Abbe refractometer AR4 (Krüss). The precision of the data reported for liquid samples is 0.001. The determination of refractive indices for complexes **1**–**8** was done using a relative method (Becke lines analysis) with a transmission light microscope Olympus BH2. For that, a crystalline sample was immersed in one of the solvent mixtures on the microscope slides. Then, the behaviour of the Becke lines was analysed in both, normal and polarised light. Whenever Becke lines changed their direction dynamic (upon increasing the focal distance) for two solvent mixtures with neighbour refractive indices, the refractive index of the analyte crystals was determined to lie between these two points. For **1** and

3–**8**, single crystals were analysed. For **2**, three microcrystalline powder samples were analysed. The precision of the refractive indices determination for solid samples is 0.01.

Absorption Spectroscopy. Reflectance spectra in the UV and visible regions have been acquired at room temperature using a Cary 5000 Series UV-Vis-NIR spectrophotometer (Agilent Technologies) equipped with a diffuse reflectance accessory Praying Mantis™ (Harrick Scientific Products) in dual beam mode using Cary WinUV software (Agilent Technologies). Powdered polytetrafluoroethylene (1 μM, Sigma-Aldrich) was used as reference material. Samples **1** and **2** were prepared and measured in air. Samples **3**–**8** were measured under Ar in an ambient chamber sample holder with a dome prepared in the glovebox. Full slit height was used for measuring samples **1** and **2**, and reduced slit height was used for measuring samples **3**–**8**. The beam alignment was checked by adjusting the light into zero-order. Both, the reference and the sample, were ground, filled into sample cups, and levelled to get a flattened surface. The lamp changeover was set at 350 nm before a background correction spectrum was recorded. For the sample, the signal intensity was maximised by increasing or decreasing the height of the sample stage. Subsequently, the sample reflectance was adjusted to 100 %R at 700 nm. The measured sample reflectance spectrum was corrected according to $\%R^{sample}_{corr} = \%R^{sample}/\%R^{reference}$.

Single Crystal X-ray Diffraction Analysis. Single crystals of the products were mounted on a goniometer head using a perfluorinated oil. All measurements were done at 100 K. Data collection was performed using Mo–Kα X-ray radiation with a BRUKER AXS D8 VENTURE (**5**, **8**, **9**, **10**, **12**, and **13**) or BRUKER AXS Apex II diffractometer with a Helios-mirror (**2**, **3**, **4**, **6**, **7**, and **11**) or a Graphite (**1**) monochromator using the BRUKER AXS Apex software package. Data processing was accomplished with XPREP. A structure solution was carried out with direct methods using SHELXT.[73] The crystal structure was refined with least square techniques using SHELXL[74] on the graphical platform shelXle.[75]

Powder X-ray Diffraction Analysis. Inside a glovebox, a sample was filled in a glass mark tube (Ø 0.3 mm, Hilgenberg GmbH), which was cut and sealed with a picein wax. Diffraction data were collected with a powder X-ray diffractometer STOE Stadi P equipped with a focusing Ge(111) monochromator and a MYTHEN 1 K strip detector (angular range 12.5° in 2θ) in a Debye-Scherrer (transmission) geometry using Cu-K_α X-ray radiation. The data collection was done in a 2θ range 5–60° with a step size of 0.015° and an integration time of 20 s. Baseline correction was performed using the BRUKER AXS DIFFRAC.EVA software.

For temperature dependant PXRD measurements, a sample was filled in a quartz mark tube (Ø 0.5 mm, Hilgenberg GmbH). Diffraction data were collected with an above-mentioned X-ray diffractometer STOE Stadi P equipped with a high-temperature furnace. The capillary opening was held under a nitrogen flow during the whole measurement. First, measurement at 25 °C was done in a 2θ range 5–50° with a step size of 0.015° and an integration time of 20 s. Then, the sample was heated up at a rate of 5 °C·min^{-1} to a desired temperature (230 °C for **1** and **2**, 270 °C for **7**, and 205 °C for **8**), which was held for an hour prior to the measurement. At high temperatures, data collection was done in a 2θ range of 4–75° with three runs with a step size of 0.015°, an offset of 0.005°, and an integration time of 20 s. For **7** and **8**, measurements at an additional high-temperature point were performed (350 °C for both, **7** and **8**), with the same temperature ramp and data collection strategy. Lastly, the sample was cooled back to 25 °C with a rate of 5 °C·min^{-1}, and the measurement at this temperature was repeated.

Thermal Analysis. Simultaneous thermogravimetry and differential thermal analysis were performed using NETZSCH STA-409-PC coupled with QMS 403 Aëolos mass spectrometer. The thermocouple temperature and sensitivity calibration was performed prior to measurements using a standard set of metals (In, Sn, Bi, Zn, Al, Ag, Au). Samples (10–20 mg) were heated up to 1000 °C with a heating rate of 5 °C·min^{-1} in an argon flow (50 mL·min^{-1}).

CHN Analysis. For CHN analysis, the compounds were placed in a tin crucible with approximately one mass equivalent of V_2O_5 (oxidation catalyst). Analyses were done with a Vario Micro Cube or Thermo FlashEA 1112 Series.

Bulk Material Syntheses

*Synthesis of α-[Eu(NO$_3$)$_3$(ptpy)(H$_2$O)] (**1**) and β-[Eu(NO$_3$)$_3$(ptpy)(H$_2$O)] (**2**)*. Mortared $Eu(NO_3)_3 \cdot 6H_2O$ (44.6 mg, 0.1 mmol) and ptpy (32.5 mg, 0.105 mmol) were mixed and placed in a Duran® culture tube. To this mixture, 1.5 mL of MeCN were added. For the analytical data presented in this manuscript, dry MeCN was used for the synthesis of **1** and **2**. The reaction was stirred at room temperature for 30 min. After that, the culture tube was centrifuged (4000 rpm, 12 min), and the solvent was removed with a syringe. Chloroform was added (1.5 mL), and the reaction mixture was stirred at room temperature for 5 minutes. The culture tube was centrifuged again, and the solvent was removed with a syringe. Afterwards, the product was dried under a vacuum at 40 °C for 20 min inside the same tube. See the discussion regarding the formation of both phases in the discussion section.

α-[Eu(NO$_3$)$_3$(ptpy)(H$_2$O)] (**1**). White powder with an intense red luminescence. Yield: 62.7 mg (94 %). Elemental analysis calculated (%) for $C_{21}H_{17}EuN_6O_{10}$: C 37.91, H 2.58, N 12.63; found: C 38.21, H 2.72, N 12.53.

β-[Eu(NO$_3$)$_3$(ptpy)(H$_2$O)] (**2**). White powder with an intense red luminescence. Yield: 65.3 mg (96 %). Elemental analysis calculated (%) for $C_{21}H_{17}EuN_6O_{10}$: C 37.91, H 2.58, N 12.63; found: C 38.02, H 2.36, N 12.43.

*Synthesis of [Eu(NO$_3$)$_3$(ptpy)(acetone)] (**3**), [Eu(NO$_3$)$_3$(ptpy)(thf)] (**4**), and [Eu(NO$_3$)$_3$(ptpy)(MeOH)] (**5**)*. Mortared $Eu(NO_3)_3 \cdot 6H_2O$ (44.6 mg, 0.1 mmol) and ptpy (32.5 mg, 0.105 mmol) were mixed and placed in a Duran® culture tube with a screw cap with a hole and a septum installed. To this mixture, 1 mL of a respective dry solvent were added (acetone for **3**, thf for **4**, MeOH for **5**). The reaction was stirred at 90 °C for 2 h. After that, the culture tube was centrifuged (4000 rpm, 12 min), and the solvent was removed with a syringe. The powder product was washed with the respective dry solvent used for the synthesis (2×1 mL) inside the reaction vessel with the help of a centrifuge. The product was dried under a vacuum at 40 °C for 20 min inside the same tube. After drying, argon was applied to the product, which was then stored in the glovebox.

[Eu(NO$_3$)$_3$(ptpy)(acetone)] (**3**). White powder with an intense red luminescence. Yield: 60.5 mg (86 %). Elemental analysis calculated (%) for $C_{24}H_{21}EuN_6O_{10}$: C 40.86, H 3.00, N 11.91; found: C 41.11, H 3.12, N 12.04.

[Eu(NO$_3$)$_3$(ptpy)(thf)] (**4**). White powder with an intense red luminescence. Yield: 62.3 mg (87 %). Elemental analysis calculated (%) for $C_{25}H_{23}EuN_6O_{10}$: C 41.74, H 3.22, N 11.68; found: C 41.83, H 3.28, N 11.72.

[Eu(NO$_3$)$_3$(ptpy)(MeOH)] (**5**). White powder with an intense red luminescence. Yield: 60.5 mg (91 %). Elemental analysis calculated (%) for $C_{22}H_{19}EuN_6O_{10}$: C 38.89, H 2.82, N 12.37; found: C 39.30, H 2.66, N 12.31.

Research Article
doi.org/10.1002/ejic.202400078

*Synthesis of [EuCl$_3$(ptpy)(acetone)] (**6**) and [EuCl$_3$(ptpy)(thf)] (**7**).* Mortared EuCl$_3$·6H$_2$O (36.6 mg, 0.1 mmol) and ptpy (32.5 mg, 0.105 mmol) were mixed and placed in a Duran® culture tube with a screw cap with a hole and a septum installed. To this mixture, 2 mL of a respective dry solvent were added (acetone for **6**, thf for **7**). The reaction was stirred at 50 °C for 16 h. After that, the culture tube was centrifuged (4000 rpm, 12 min), and the solvent was removed with a syringe. The powder product was washed with the respective dry solvent used for the synthesis (2×1 mL) inside the reaction vessel with the help of a centrifuge. The product was dried under a vacuum at 40 °C for 20 min inside the same tube. After drying, argon was applied to the product, which was then stored in the glovebox.

[EuCl$_3$(ptpy)(acetone)] (**6**): White powder with an intense red luminescence. Yield: 61.8 mg (99%). Elemental analysis calculated (%) for C$_{24}$H$_{21}$Cl$_3$EuN$_3$O: C 46.07, H 3.38, N 6.72; found: C 45.98, H 3.70, N 6.50.

[EuCl$_3$(ptpy)(thf)] (**7**): White powder with an intense red luminescence. Yield: 61.9 mg (97%). Elemental analysis calculated (%) for C$_{25}$H$_{23}$Cl$_3$EuN$_3$O: C 46.93, H 3.62, N 6.57; found: C 47.04, H 3.81, N 6.49.

*Synthesis of [EuCl$_3$(ptpy)(MeOH)] (**8**).* EuCl$_3$·6H$_2$O (36.6 mg, 0.1 mmol) and ptpy (31.5 mg, 0.102 mmol) were placed together in a Duran® culture tube with a screw cap with a hole and a septum installed. To this mixture, 2 mL of dry MeOH were added. The reaction was stirred at 90 °C for 2 h. After that, the culture tube was centrifuged (4000 rpm, 12 min), and the solvent was removed with a syringe. The powder product was dried under vacuum at 40 °C for 20 min inside the same tube. After drying, argon was applied to the product, which was then stored in the glovebox. The product was obtained as a white powder with an intense red luminescence. Yield: 24.5 mg (41%). Elemental analysis calculated (%) for C$_{22}$H$_{19}$Cl$_3$EuN$_3$O: C 44.06, H 3.19, N 7.01; found: C 44.64, H 3.05, N 7.19.

Single Crystal Syntheses

*Synthesis of single crystals of α-[Eu(NO$_3$)$_3$(ptpy)(H$_2$O)] (**1**).* α-[Eu(NO$_3$)$_3$(ptpy)(H$_2$O)] (**5**, 20 mg, 0.03 mmol) was dissolved in MeCN (9 mL). The solution was left open to the air for evaporation. After one week, single crystals with a red luminescence were formed, and they were dried and analysed.

*Synthesis of single crystals of β-[Eu(NO$_3$)$_3$(ptpy)(H$_2$O)] (**2**).* Eu(NO$_3$)$_3$·6H$_2$O (4.5 mg, 0.01 mmol) was dissolved in MeCN (1 mL) and ptpy (3 mg, 0.01 mmol) was dispersed in MeCN (1 mL). Prepared solution and dispersion were mixed. After 2 h, Et$_2$O (1 mL) was added. After 6 h, cyclohexane (1 mL) was added. After three days, the mixture was left open to the air for evaporation. In 10 days, single crystals with a red luminescence were formed. They were dried and analysed.

*Synthesis of single crystals of [Eu(NO$_3$)$_3$(ptpy)(acetone)] (**3**).* Eu(NO$_3$)$_3$·6H$_2$O (4.5 mg, 0.01 mmol) and ptpy (3.4 mg, 0.011 mmol) were sealed together with acetone (0.1 mL) in an ampoule. It was heated in a resistance heating glass oven Büchi B-585 at 85 °C for 65 h. Afterwards, the ampoule was unsealed, and the solvent was removed with a syringe. Crystals with an intense red luminescence were washed with toluene (2×1 mL) and analysed.

*Synthesis of single crystals of [Eu(NO$_3$)$_3$(ptpy)(thf)] (**4**).* Eu(NO$_3$)$_3$·6H$_2$O (4.5 mg, 0.01 mmol) and ptpy (3.4 mg, 0.011 mmol) were sealed together with tetrahydrofuran (0.2 mL) in an ampoule. It was heated in a resistance heating glass oven Büchi B-585 at 80 °C for 64 h. Afterwards, the ampoule was unsealed, and the solvent was removed with a syringe. Crystals with an intense red luminescence were analysed.

*Synthesis of single crystals of [Eu(NO$_3$)(ptpy)(MeOH)] (**5**).* α-[Eu(NO$_3$)$_3$(ptpy)(H$_2$O)] (**5**, 2 mg, 0.003 mmol) together with MeOH (0.5 mL) were sealed in an ampoule. It was heated in a resistance heating glass oven Büchi B-585 at 100 °C for 48 h. Afterwards, the ampoule was unsealed, and the solvent was removed with a syringe. Crystals with an intense red luminescence were analysed.

*Synthesis of single crystals of [EuCl$_3$(ptpy)(acetone)] (**6**).* EuCl$_3$·6H$_2$O (3.6 mg, 0.01 mmol) and ptpy (4.6 mg, 0.015 mmol) were sealed together with acetone (0.5 mL) in an ampoule. It was heated in a resistance heating oven at 120 °C for 144 h. Afterwards, the ampoule was unsealed, and the solvent was removed with a syringe. Crystals with an intense red luminescence were washed with toluene (2×1.5 mL) and analysed.

*Synthesis of single crystals of [EuCl$_3$(ptpy)(thf)] (**7**).* EuCl$_3$·6H$_2$O (3.6 mg, 0.01 mmol) and ptpy (4.6 mg, 0.015 mmol) were sealed together with tetrahydrofuran (0.5 mL) in an ampoule. It was heated in a resistance heating oven at 120 °C for 96 h. Afterwards, the ampoule was unsealed, and the solvent was removed with a syringe. Crystals with an intense red luminescence were washed with toluene (2×1.5 mL) and analysed.

*Synthesis of single crystals of [EuCl$_3$(ptpy)(MeOH)] (**8**).* EuCl$_3$·6H$_2$O (3.6 mg, 0.01 mmol) and ptpy (3.4 mg, 0.011 mmol) were sealed together with MeOH (0.3 mL) in an ampoule. It was heated in a resistance heating oven at 130 °C for 16 h and then at 140 °C for 164 h. Afterwards, the ampoule was unsealed, and the solvent was removed with a syringe. Crystals with an intense red luminescence were analysed.

*Synthesis of single crystals of [Eu(NO$_3$)$_3$(ptpy)(MeCN)] (**9**) and [Eu$_2$(NO$_3$)$_6$(ptpy)$_2$] (**10**).* α-[Eu(NO$_3$)$_3$(ptpy)(H$_2$O)] (**1**, 3.3 mg, 0.005 mmol) was sealed together with acetonitrile (0.3 mL) in an ampoule. It was heated in a resistance heating glass oven Büchi-585 at 100 °C for three weeks. Afterwards, the ampoule was unsealed, and the solvent was removed with a syringe. Crystals with a red luminescence were analysed.

*Synthesis of single crystals of [Eu(NO$_3$)$_3$(ptpy)(H$_2$O)]·thf (**11**).* Eu(NO$_3$)$_3$·6H$_2$O (4.5 mg, 0.01 mmol) and ptpy (3.4 mg, 0.011 mmol) were sealed together with tetrahydrofuran (0.1 mL) in an ampoule. It was heated in a resistance heating glass oven Büchi B-585 at 50 °C for three weeks. Then, it was heated at 60 °C for two days and at 80 °C for four days. Afterwards, the ampoule was unsealed, and the solvent was removed with a syringe. Crystals with a red luminescence were analysed.

*Synthesis of single crystals of [EuCl$_3$(ptpy)(H$_2$O)(MeOH)] (**12**).* EuCl$_3$·6H$_2$O (3.6 mg, 0.01 mmol) and ptpy (3.4 mg, 0.011 mmol) were sealed together with MeOH (0.1 mL) in an ampoule. It was heated in a resistance heating glass oven Büchi B-585 at 50 °C for three weeks. Afterwards, the ampoule was unsealed, and the solvent was removed with a syringe. Crystals with a red luminescence were analysed.

*Synthesis of single crystals of [EuCl$_2$(ptpy)$_2$]Cl·2MeOH (**13**).* [EuCl$_3$(ptpy)(MeOH)] (**8**, 20 mg, 0.033 mmol) was sealed together with 0.2 mL of MeOH in an ampoule. It was heated in a resistance heating glass oven Büchi B-585 at 60 °C for 43 h. Afterwards, the ampoule was unsealed, and the solvent was removed with a syringe. Crystals with a red luminescence were analysed.

Acknowledgements

The authors gratefully acknowledge the Deutsche Forschungsgemeinschaft for supporting this work within the project MU-1562/16-1 and the Justus-Liebig University Giessen for a knock-on financing and general support. The authors acknowledge Stephanie Maaß (Julius-Maximilians-University of Würzburg) for the synthesis of 4′-phenyl-2,2′:6′,2″-terpyridine. Open Access funding enabled and organized by Projekt DEAL.

Conflict of Interests

The authors declare no conflict of interest.

Data Availability Statement

The data is uploaded to the public repository of Justus-Liebig-University of Giessen (JLUpub), the DOI has been assigned. This is indicated in the main text of the document with the DOI provided.

Keywords: analytical methods · lanthanides · luminescence · N ligands · solid-state structures

[1] F. C. Goerigk, S. Schander, M. S. Wickleder, T. Schleid, *Z. Anorg. Allg. Chem.* **2020**, *646*, 985–991.
[2] M. Ben Hamida, M. S. Wickleder, *Z. Anorg. Allg. Chem.* **2006**, *632*, 2195–2197.
[3] P. A. Tanner, Y. Y. Yeung, L. Ning, *J. Phys. Chem. A* **2013**, *117*, 2771–2781.
[4] B. Golesorkhi, S. Naseri, L. Guénée, I. Taarit, F. Alves, H. Nozary, C. Piguet, *J. Am. Chem. Soc.* **2021**, *143*, 15326–15334.
[5] H. Bolvin, A. Fürstenberg, B. Golesorkhi, H. Nozary, I. Taarit, C. Piguet, *Acc. Chem. Res.* **2022**, *55*, 442–456.
[6] Y. Suffren, B. Golesorkhi, D. Zare, L. Guénée, H. Nozary, S. V. Eliseeva, S. Petoud, A. Hauser, C. Piguet, *Inorg. Chem.* **2016**, *55*, 9964–9972.
[7] R. J. Batrice, A. K. Adcock, P. M. Cantos, J. A. Bertke, K. E. Knope, *Cryst. Growth Des.* **2017**, *17*, 4603–4612.
[8] M. A. Zhernakov, A. E. Sedykh, J. Becker, M. Maxeiner, K. Müller-Buschbaum, V. G. Shtyrlin, *Z. Anorg. Allg. Chem.* **2022**, *648*, e202200230.
[9] V. K. Gramm, A. Schuy, M. Suta, C. Wickleder, C. Sternemann, U. Ruschewitz, *Z. Anorg. Allg. Chem.* **2018**, *644*, 127–135.
[10] A. E. Kalugin, M. E. Minyaev, L. N. Puntus, I. V. Taydakov, E. A. Varaksina, K. A. Lyssenko, I. E. Nifant'ev, D. M. Roitershtein, *Molecules* **2020**, *25*, 3934.
[11] R. Ilmi, J. Wang, J. D. L. Dutra, L. Zhou, W. Wong, P. R. Raithby, M. S. Khan, *Chem. Eur. J.* **2023**, *29*, e202300376.
[12] R. J. Batrice, R. L. Ayscue, A. K. Adcock, B. R. Sullivan, S. Y. Han, P. M. Piccoli, J. A. Bertke, K. E. Knope, *Chem. Eur. J.* **2018**, *24*, 5630–5636.
[13] G. E. Gomez, C. A. López, R. L. Ayscue, K. E. Knope, M. D. R. Torres Deluigi, G. E. Narda, *Dalton Trans.* **2019**, *48*, 12080–12087.
[14] I. A. Razumkova, A. E. Sedykh, Y. G. Denisenko, K. Müller-Buschbaum, *J. Ind. Eng. Chem.* **2020**, *92*, 218–225.
[15] A. Mattner, L. Zimmermann, S. Lienenklaus, S. Weiss, C. Wickleder, *Ceram. Int.* **2020**, *46*, 26295–26298.
[16] A. M. Kaczmarek, M. Suta, H. Rijckaert, T. P. van Swieten, I. Van Driessche, M. K. Kaczmarek, A. Meijerink, *J. Mater. Chem. C* **2021**, *9*, 3589–3600.
[17] E. Regalado-Pérez, N. R. Mathews, X. Mathew, *Sol. Energy* **2020**, *199*, 82–91.
[18] T. Fiedler, M. Hilder, P. C. Junk, U. H. Kynast, M. M. Lezhnina, M. Warzala, *Eur. J. Inorg. Chem.* **2007**, *2007*, 291–301.
[19] X. Li, J. Gu, Z. Zhou, L. Ma, Y. Tang, J. Gao, Q. Wang, *Chem. Eng. J.* **2019**, *358*, 67–73.
[20] K. Lunstroot, K. Driesen, P. Nockemann, L. Viau, P. H. Mutin, A. Vioux, K. Binnemans, *Phys. Chem. Chem. Phys.* **2010**, *12*, 1879–1885.
[21] S. Ullmann, P. Hahn, P. Mini, K. L. Tuck, A. Kahnt, B. Abel, M. E. Gutierrez Suburu, C. A. Strassert, B. Kersting, *Dalton Trans.* **2020**, *49*, 11179–11191.
[22] L. Armelao, S. Quici, F. Barigelletti, G. Accorsi, G. Bottaro, M. Cavazzini, E. Tondello, *Coord. Chem. Rev.* **2010**, *254*, 487–505.
[23] J.-C. G. Bünzli, *Coord. Chem. Rev.* **2015**, *293–294*, 19–47.
[24] K. L. Wong, J. C. G. Bünzli, P. A. Tanner, *J. Lumin.* **2020**, *224*, 117256.
[25] K. Binnemans, *Coord. Chem. Rev.* **2015**, *295*, 1–45.
[26] J. Petry, R. Komban, C. Gimmler, H. Weller, *Nanoscale Adv.* **2022**, *4*, 858–864.
[27] J. P. Martins, P. Martín-Ramos, C. Coya, M. R. Silva, M. E. S. Eusebio, A. de Andrés, Á. L. Álvarez, J. Martín-Gil, *J. Lumin.* **2015**, *159*, 17–25.
[28] R. Devi, S. Vaidyanathan, *Dalton Trans.* **2020**, *49*, 6205–6219.
[29] R. Boddula, J. Tagare, K. Singh, S. Vaidyanathan, *Mater. Chem. Front.* **2021**, *5*, 3159–3175.
[30] K. Singh, R. Boddula, S. Vaidyanathan, *Inorg. Chem.* **2017**, *56*, 9376–9390.
[31] R. Devi, M. Rajendran, K. Singh, R. Pal, S. Vaidyanathan, *J. Mater. Chem. C* **2021**, *9*, 6618–6633.
[32] J. Wu, X. Zhou, D. Zhang, L. Li, S. Jiang, G. Xiang, Y. Wang, X. Tang, J. Li, Z. Cao, *J. Lumin.* **2023**, *257*, 119686.
[33] O. Moudam, O. Lakbita, *ACS Omega* **2021**, *6*, 29659–29663.
[34] Y. Jia, Z. Shi, J. Wang, X. Li, Z. Zhao, *J. Lumin.* **2023**, *253*, 119489.
[35] J. F. Suyver, A. Meijerink, *Chemisch2Weekblad* **2002**, *98*, 12–13.
[36] C. D. S. Brites, R. Marin, M. Suta, A. N. Carneiro Neto, E. Ximendes, D. Jaque, L. D. Carlos, *Adv. Mater.* **2023**, *35*, 202302749.
[37] A. Carlotto, L. Babetto, S. Carlotto, M. Miozzi, R. Seraglia, M. Casarin, G. Bottaro, M. Rancan, L. Armelao, *ChemPhotoChem* **2020**, *4*, 674–684.
[38] T. Miyagawa, T. Fujie, Ferdinandus, T. T. Vo Doan, H. Sato, S. Takeoka, *ACS Appl. Mater. Interfaces* **2016**, *8*, 33377–33385.
[39] Ferdinandus, S. Arai, S. Takeoka, S. Ishiwata, M. Suzuki, H. Sato, *ACS Sens.* **2016**, *1*, 1222–1227.
[40] L. Chen, Y. Zhang, A. Luo, F. Liu, Y. Jiang, Q. Hu, S. Chen, R. Liu, *Phys. Status Solidi RRL* **2012**, *6*, 321–323.
[41] M. H. V. Werts, R. T. F. Jukes, J. W. Verhoeven, *Phys. Chem. Chem. Phys.* **2002**, *4*, 1542–1548.
[42] B. R. Judd, *Phys. Rev.* **1962**, *127*, 750–761.
[43] G. S. Ofelt, *J. Chem. Phys.* **1962**, *37*, 511–520.
[44] J. C. G. Bünzli, A. S. Chauvin, H. K. Kim, E. Deiters, S. V. Eliseeva, *Coord. Chem. Rev.* **2010**, *254*, 2623–2633.
[45] L. L. Cai, Y. T. Hu, Y. Li, K. Wang, X. Q. Zhang, G. Muller, X. M. Li, G. X. Wang, *Inorg. Chim. Acta* **2019**, *489*, 85–92.
[46] N. M. Shavaleev, F. Gumy, R. Scopelliti, J.-C. G. Bünzli, *Inorg. Chem.* **2009**, *48*, 5611–5613.
[47] N. M. Shavaleev, S. V. Eliseeva, R. Scopelliti, J. C. G. Bünzli, *Chem. Eur. J.* **2009**, *15*, 10790–10802.
[48] S. V. Eliseeva, D. N. Pleshkov, K. A. Lyssenko, L. S. Lepnev, J.-C. G. Bünzli, N. P. Kuzmina, *Inorg. Chem.* **2011**, *50*, 5137–5144.
[49] Y. Hasegawa, S. Natori, J. Fukudome, T. Nagase, T. Kobayashi, T. Nakanishi, Y. Kitagawa, K. Fushimi, H. Naito, *J. Phys. Chem. C* **2018**, *122*, 9599–9605.
[50] P. Dhankhar, R. Devi, S. Devi, S. Chahar, M. Dalal, V. B. Taxak, S. P. Khatkar, P. Boora, *Rare Met.* **2022**, *41*, 1342–1352.
[51] F. S. M. Canisares, A. M. G. Mutti, D. G. S. M. Cavalcante, A. E. Job, A. M. Pires, S. A. M. Lima, *J. Photochem. Photobiol. A* **2022**, *422*, 113552.
[52] E. V. Salerno, S. V. Eliseeva, B. L. Schneider, J. W. Kampf, S. Petoud, V. L. Pecoraro, *J. Phys. Chem. A* **2020**, *124*, 10550–10564.
[53] O. T. Alexander, R. E. Kroon, A. Brink, H. G. Visser, *Dalton Trans.* **2019**, *48*, 16074–16082.
[54] N. E. Borisova, A. V. Ivanov, A. V. Kharcheva, T. B. Sumyanova, U. V. Surkova, P. I. Matveev, S. V. Patsaeva, *Molecules* **2019**, *25*, 62.
[55] R. Boddula, S. Vaidyanathan, *Inorg. Chim. Acta* **2019**, *494*, 141–153.
[56] A. E. Sedykh, D. G. Kurth, K. Müller-Buschbaum, *Eur. J. Inorg. Chem.* **2019**, *2019*, 4564–4571.
[57] A. E. Sedykh, R. Bissert, D. G. Kurth, K. Müller-Buschbaum, *Z. Kristallogr.* **2020**, *235*, 353–363.
[58] R. C. Faust, *Proc. Phys. Soc. London Sect. B* **1955**, *68*, 1081–1094.
[59] M. Manutchehr-Danai, *Becke line method in Dictionary of Gems and Gemology*, Springer Berlin Heidelberg, Berlin, Heidelberg, **2009**, p. 77.
[60] J.-C. G. Bünzli, S. V. Eliseeva, *Basics of Lanthanide Photophysics in Lanthanide Luminescence*, **2010**, pp. 1–45.
[61] M. Latva, H. Takalo, V.-M. Mukkala, C. Matachescu, J. C. Rodríguez-Ubis, J. Kankare, *J. Lumin.* **1997**, *75*, 149–169.
[62] A. E. Sedykh, D. G. Kurth, K. Müller-Buschbaum, *Z. Anorg. Allg. Chem.* **2021**, *647*, 359–364.
[63] A. Ruiz-Martínez, S. Alvarez, *Chem. Eur. J.* **2009**, *15*, 7470–7480.

Research Article
doi.org/10.1002/ejic.202400078

[64] C. Spangler, M. Schäferling, *Luminescent Chemical and Physical Sensors Based on Lanthanide Complexes in Lanthanide Luminescence*, **2010**, pp. 235–262.
[65] P. D. I. Fletcher, R. J. Nicholls, *Langmuir* **2000**, *16*, 1050–1056.
[66] M. Bagheri, F. Kiani, F. Koohyar, N. T. Khang, F. Zabihi, *J. Mol. Liq.* **2020**, *309*, 113109.
[67] C. Wohlfarth, *Optical Constants: Refractive Indices of Pure Liquids and Binary Liquid Mixtures (Supplement to III/38)*, **2008**.
[68] S. S. Batsanov, E. D. Ruchkin, I. A. Poroshina, *Anisotropy, Dispersion, Theory and Structural Effects in Refractive Indices of Solids*, **2016**, pp. 3–7.
[69] J. Wang, G. Hanan, *Synlett* **2005**, *2005*, 1251–1254.
[70] M. S. Wrighton, D. S. Ginley, D. L. Morse, *J. Phys. Chem.* **1974**, *78*, 2229–2233.
[71] S. Balabhadra, M. L. Debasu, C. D. S. Brites, R. A. S. Ferreira, L. D. Carlos, *J. Lumin.* **2017**, *189*, 64–70.
[72] A. E. Sedykh, M. Becker, M. T. Seuffert, D. Heuler, M. Maxeiner, D. G. Kurth, C. E. Housecroft, E. C. Constable, K. Müller-Buschbaum, *ChemPhotoChem* **2023**, *7*, e202200244.
[73] G. M. Sheldrick, *Acta Crystallogr. Sect. A* **2015**, *71*, 3–8.
[74] G. M. Sheldrick, *Acta Crystallogr. Sect. C* **2015**, *71*, 3–8.
[75] C. B. Hübschle, G. M. Sheldrick, B. Dittrich, *J. Appl. Crystallogr.* **2011**, *44*, 1281–1284.

Manuscript received: February 6, 2024
Revised manuscript received: April 8, 2024
Accepted manuscript online: April 10, 2024
Version of record online: May 13, 2024